

## Stockholm University

This is a submitted version of a paper published in *Astrophysical Journal*.

Citation for the published paper:

Mahmood, S., Ali, S., Orban, I., Tashenov, S., Lindroth, E. et al. (2012)

"Recombination and electron impact excitation rate coefficients for S XV AND S XVI"

*Astrophysical Journal*, 754(2): 86

URL: <http://dx.doi.org/10.1088/0004-637X/754/2/86>

Access to the published version may require subscription.

Permanent link to this version:

<http://urn.kb.se/resolve?urn=urn:nbn:se:su:diva-75369>



<http://su.diva-portal.org>

# RECOMBINATION AND ELECTRON IMPACT EXCITATION RATE COEFFICIENTS FOR S XV AND S XVI

S. MAHMOOD, S. ALI, I. ORBAN, S. TASHENOV\*, E. LINDROTH, AND R. SCHUCH

Department of Physics, Stockholm University, AlbaNova University Center S-10691 Stockholm, Sweden

## ABSTRACT

Recombination and electron impact excitation of  $S^{14+}$  and  $S^{15+}$  ions was measured at the Stockholm refrigerated electron beam ion trap. The collision energy range was 1.4-3 keV, where we covered the KLL, KLM, KLN, and KLO dielectronic recombination resonances resulting in  $S^{13+}$  and  $S^{14+}$  ions. The recombination rates were obtained by detecting the charge state distribution with a newly developed time-of-flight technique. Resonance energies and cross sections calculated within the relativistic many-body perturbation theory for  $S^{15+}$  agree well with the experimental data. The temperature dependent rate coefficients have been extracted from the measured rates and compared with calculations from literature used for studies of collisionally ionized astrophysical plasmas. A good agreement for  $S^{15+}$  was obtained, while the plasma rates for  $S^{14+}$  were 23 % lower than the so far published values. In addition to the time-of-flight spectra, the x-ray spectra, produced mainly by photo-recombination and excitation, have been also collected. The combination of these two measurements allowed us to separate the photo-recombination and the excitation spectra, and the excitation rate coefficients for summed intensities with known fractions of  $S^{14+}$  and  $S^{15+}$  ions were extracted.

Key words: atomic data - atomic processes - plasmas

## 1. INTRODUCTION

The charge state distributions in a plasma are governed by several atomic processes, of which electron impact processes are particularly important (Ferland et al. 1998; Smith et al. 2001). These processes include electron impact ionization (EII) (Dere 2007), electron impact excitation (EIE) (Zhang & Sampson 1987), and electron-ion recombination (Mazzotta et al. 1998). The relevant rate coefficients are thus needed for astrophysical and laboratory plasma modelling. For example recombination accompanied by the emission of photons plays a crucial role for plasma diagnostics (Gabriel & Jordan 1973; Porquet et al. 2001). Dielectronic recombination (DR) in particular, is a source of characteristic x-ray emission, e.g. from the solar corona (Dubau & Volonte 1980; Khan, et al. 1995). It is in general of great importance for atomic physics (Müller 2009), nuclear physics (Schuch et al. 2005), and astrophysics (Burgess & Summers 1969; Kallman & Palmeri 2007). DR is a resonant two step process which occurs in non-bare ions. In the first step, the capture of a free electron into an excited state of the ion is accompanied by the excitation of a bound electron. In the second step this doubly-excited state decays radiatively or by autoionization. While autoionization leaves the ion in the original charge state, radiative decay to states below the ionization threshold of the recombined system completes DR and the charge state of the ion decreases by one.

Information about various physical conditions and processes occurring in astrophysical objects is extracted from the ionic spectral lines emitted during DR. In collisionally ionized plasmas H-like and He-like ions are of particular interest as line ratios of their radiative transitions can be used for plasma diagnostics and reliable data is needed for these isoelectronic sequences. Foster et al. 2010 show the effects of uncertainties in atomic data on derived temperature and density of plasma. The plasma modelling requires vast quantities of atomic data. For each ion one needs energy levels as well as excitation, ionization, recombination, and photoemission cross sections. For modelling collisionally ionized plasma one uses frequently atomic databases such as XSPEC (Arnaud 1996), CHIANTI (Dere et al. 2009), ADAS (Summers 2010), and AtomDB (Smith & Foster 2010). The recommended recombination rate coefficients are updated by Bryans et al. 2006. The recombination data for sulfur ions used in these codes was so far obtained from calculations.

Sulfur is produced as a product of the oxygen-burning fusion process in stellar nucleosynthesis (Clayton 1983; Woosley et al. 2002). Thus it is present in most of astrophysical plasmas. The observations by Chandra and XMM-Newton x-ray observatories have shown the existence of sulfur ions in astrophysical objects. The emissions lines from highly charged sulfur ions have been observed

---

\*□ Present address : Physikalisches Institut, Universität Heidelberg, D-69120 Heidelberg, Germany

with Chandra from x-ray binaries such as SS 433 (Marshall et al. 2002), 4U 1700-37 (Boroson et al. 2003), and Cir X-1 (Iaria et al. 2008). Decourchelle et al. (2001) reported occurrence of sulfur ions in Tycho supernova remnant based on an observation obtained with XMM-Newton. The observations of the supernova remnant W49B by ASCA (Fujimoto et al. 1995) and XMM-Newton (Miceli et al. 2006) revealed the K shell emission lines from sulfur ions. K x-rays originating from sulfur ions were also observed from stars (Wojdowski et al. 2003), Eta Carinae (Henley et al. 2008), and clusters of galaxies (Sarazin 1988). Sterling et al. (1997) derived the electron temperatures of the sun's corona (AR 7978) from the spectra of He-like sulfur ions. The future x-ray missions e.g. Astro-H will probe higher temperature and dense astrophysical plasmas where the data for high Z ions e.g. S, Ca, Fe and Ni are needed (Porquet et al. 2010). Here we also selected sulfur due to its high abundance in the solar system (Anders & Grevesse 1989, Grevesse & Sauval 1998). Sulfur dominates the surface of Jupiter's satellite Io (Postberg et al. 2006). Hot plasmas were observed in its magnetosphere with particles moving with up to 10 % of the speed of light and thus capable of sulfur ionization until the highest charge states. Until the presented measurements, no published experimental recombination data was available for H-like and He-like sulfur ions. Previous work on  $S^{15+}$  ions was shown in an internal report (Wolf 1992), but not in an accessible journal.

Recombination studies of highly charged ions have been performed at storage rings (Kilgus et al. 1990; see also the reviews by Schuch & Böhm 2007 and Müller 2009) and at Electron beam Ion Traps (EBIT) and sources (Levine et al. 1989; Knapp et al. 1989; Ali et al. 1990; Biedermann et al. 1997; Watanabe et al. 2001; Zou et al. 2003; Böhm et al. 2007). In storage ring experiments, the electron beam is merged with the stored ions and in most cases the charge changed ions are detected. The storage rings are typically used for low energy (meV-100 eV) electron-ion recombination measurements. In an EBIT, a high-density electron beam interacts with the ions confined in a trap and electron-ion collisions are investigated in the energy range from typically 100 eV to a few hundred keV.

Recombination and EIE studies at EBITs are usually performed by detecting photons emitted by the trapped ions. When solid state detectors, such as Si(Li) and HPGe detectors, are used to acquire the energy spectra, the photon emission lines from different charge states often overlap. This prevents extraction of the charge selective recombination rate coefficients. In contrast to that, the energy resolution of crystal spectrometers and microcalorimeters is sufficient to distinguish photon emission from different charge states. Crystal spectrometers have, however, a low efficiency; in addition their measured photon intensity depends on photon polarization. Microcalorimeters have both high resolution and high quantum efficiency but they currently can only cover small solid angles. Therefore in the last two cases long measurement times are typically required. So far all the photon detection methods using an EBIT are affected by the anisotropy of the emitted radiation and this needs to be accounted for.

Recombination measurements can also be performed by detecting the charge distribution of ions extracted from the trap. In one of the methods the ion content of the trap is analyzed by detecting the ions escaping over the trap potential as a function of the electron beam energy (Watanabe et al. 2007). For these measurements, it is assumed that the number of escaping ions is proportional to the ion abundance in the trap. Alternatively, the charge state distribution can be measured by opening the trap and extracting all the trapped ions (Ali et al. 1990; DeWitt et al. 1991). So far, the charge analysis of the extracted ions was done by a dipole magnet. With this method only a few charge states can be detected simultaneously. We introduced a new approach in which the entire ion cloud is extracted from the EBIT in a short pulse and the ions of different charges ( $Q$ ) and masses ( $m$ ) are separated by their time-of-flight (TOF) before they arrive at the detector (Orban et al. to be published). With this technique the complete  $m/Q$  spectrum is obtained for every extraction, which allows us to monitor all charge states simultaneously.

In this paper we report on DR rate coefficients for H-like and He-like sulfur ions obtained with the TOF technique. With these data the temperature dependent DR rate coefficients were calculated for plasmas with Maxwell-Boltzmann electron energy distribution. Additionally we measured the photons, emitted from the trapped ions in the same run of the R-EBIT under identical experimental conditions (Ali et al. 2011a). Using the combination of the TOF and x-ray spectra, the excitation rate coefficients for summed intensities with known fractions of  $S^{14+}$  and  $S^{15+}$  ions were obtained. For labelling of the DR resonances we use the Auger notation and indicate the ion charge state before recombination.

## 2. EXPERIMENT

The measurements were performed at the Stockholm Refrigerated Electron Beam Ion Trap (R-EBIT) (Böhm et al. 2007). In the R-EBIT, the electron beam energy is determined by the potential applied to cathode and drift tube assembly of the trap. In the trap region the electron beam is compressed to a radius of 35  $\mu\text{m}$  by a magnetic field of 3 T from a superconducting magnet, creating a typical density of  $10^{11}$  electrons/cm<sup>3</sup>. As electrons advance through the drift tube assembly, they ionize SH<sub>2</sub> gas injected in the trap region using a pulsed gas-injection system (Hobein et al. 2010).

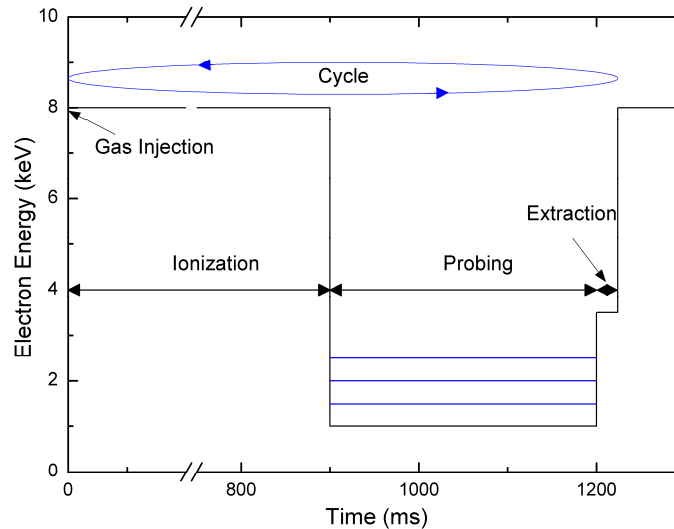


Figure 1. The R-EBIT time cycle of switching the electron beam energy used for the recombination measurement.

Along the electron beam direction, the ions are trapped in the potential well, created by higher positive potentials of the outer drift tubes with respect to the potential of the middle drift tube. The potential difference between the extraction and the middle drift tube defined the trap depth of 8.5 V. Transversally, the ions are confined by the combination of the strong magnetic field and the space charge of the electron beam. The residual gas pressure in the cryogenic trap could not be directly measured. The pressure in the R-EBIT tank was monitored to be constant. Moreover, a pressure variation in the R-EBIT would have influenced the ion abundances and that was not observed.

In order to prepare the ions, probe the recombination rate, and extract the ion cloud into the TOF spectrometer, the potential of the drift tube assembly was alternated in a cycle throughout the experiment, see Figure 1. It contains a sequence of charge breeding, probing, and extraction intervals. During the ionization time, the electron beam energy was set to 8 keV for 900 ms in order to produce the initial charge state distribution of the sulfur ions. The distribution was concentrated around the highest charge states peaking at He-like ions. After charge breeding, the ions were probed at fixed electron beam energy for 300 ms. This energy was incremented by 4 eV in each successive cycle and in this way the 1.4-3 keV electron-ion interaction energy range was scanned. During the experiment, the electron beam current was set to 10 mA. This allowed for the optimum combination of the energy resolution, limited by the electron beam space charge, and the count rate, limited by the electron beam density and the number of trapped ions.

Shortly before the extraction, the potential on the drift tube assembly was set to 3.5 kV. This potential was chosen for optimal ion extraction, transportation, and TOF resolution. After probing, the ions were extracted from the R-EBIT by decreasing the potential of the extraction drift tube below the potential of the middle drift tube in a time interval of < 100 ns. Following a flight path of 3 meters through a straight beam line, the extracted ions were detected by an open electron multiplier connected to a fast digital oscilloscope. The pulse shapes triggered by the extraction signal and recorded by the oscilloscope represent the TOF spectrum of the extracted ions. The digitized TOF spectra for each cycle were stored by a LabView acquisition program along with the probing electron energy.

The X rays emitted by the trapped ions were also measured during the probing time. This was done by a Si(Li) detector placed perpendicular to the electron beam direction, at an observational port of R-EBIT (Ali et al. 2011a). A LabView-based data acquisition system recorded x-ray data in event mode and was also used to control the electron beam energy (Ali et al. 2011b).

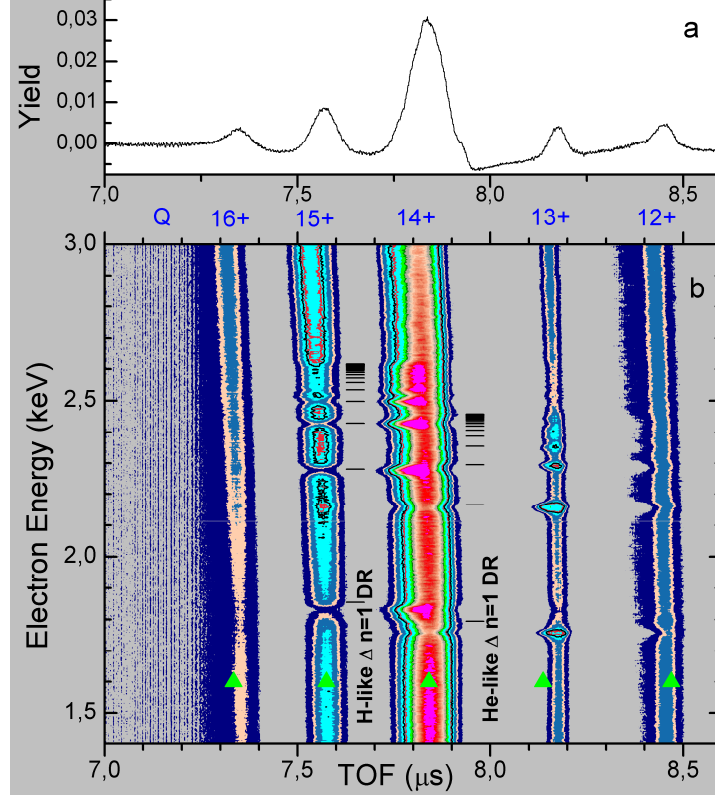


Figure 2. a) The TOF spectrum of the extracted ion cloud following the probing interval with the electron energy of 2.1 keV. b) The TOF spectrum as a function of the probing electron energy. The green triangles show the calculated TOF values and  $Q$  denotes the charge state of the sulfur ions. The horizontal bars are the estimated DR resonance energy positions.

### 3. RESULTS AND DISCUSSION

A typical TOF spectrum is shown in Figure 2a for the probing energy of 2.1 keV. The well resolved peaks correspond to extracted ion bunches of a particular  $m/Q$  with the intensities proportional to the numbers of ions. It thus directly reflects the charge state distribution right after the probing period. This spectrum as a function of the probing electron energy is shown in Figure 2b. The TOF spectrum is the average of 48 measurements at each probing energy. The charge states of sulfur ions after probing are indicated on the upper abscissa. It is also observed that the TOF increases slowly at the lower electron energies. This effect has a technical origin: the high voltage supply for the drift tube assembly did not have enough time to stabilize after switching from the probing to the extraction potential. However, this did not affect the measurement of the charge state distribution.

The probing electron energy of 1.4-3 keV was selected to lie below the ionization threshold of 3.494 keV for  $S^{15+}$  ions. The charge changing reactions therefore included radiative recombination (RR), DR and charge exchange with neutral atoms and molecules. The effect of RR is apparent in the gradual decrease of the abundance of bare ions for lower electron energies. The abrupt variations in the peak intensities correspond to DR resonances. This resonance-like structure is observed for all charge states except for the bare ions. The resonance energies can be estimated using the following formula

$$E_e = E_{\text{exc}} - E_b(nl) = E_{\text{exc}} - Ry \left( \frac{Q}{n} \right)^2 [\text{eV}], \quad (1)$$

where  $E_e$  is the energy of the incident electron,  $E_{\text{exc}}$  is the excitation energy of the core electron in initial system, and  $E_b(nl)$  is the binding energy of the outer electron in the doubly excited state.  $E_b(nl)$  is estimated with the Rydberg formula using the ion charge state  $Q$ , Rydberg constant  $Ry$ , and the principal quantum number  $n$  (neglecting the quantum defects of different angular momentum  $\ell$  states). The horizontal bars in Figure 2b, show the estimated DR resonance energies for H-like and He-like ions, calculated using equation 1.

The TOF of different charge species, calculated for a neglected ion space charge potential, agrees well with the measured values, see Figure 2b, green triangles. The deviation of TOF for the  $S^{13+}$  ion bunch from the prediction is caused by the high space charge of the neighboring bunch of the more abundant  $S^{14+}$  ions. It screens the accelerating extraction potential for  $S^{13+}$  ions thus slowing them down. This effect is further pronounced by the shifts of the TOF at DR resonances. The abrupt changes of the abundance of the neighboring ions result in either a decrease or increase of the ion velocity depending on whether the neighboring bunch moves in front of or behind the affected ions. As an example, in the case of the first DR resonance at 1.75 keV (KLL DR of He-like ions), the number of  $S^{14+}$  ions decreased, leading to a reduced screening of the accelerating potential for the  $S^{13+}$  ions. Thus, the  $S^{13+}$  ions reach the detector at an earlier time, as compared to the off-resonance electron energies. The increased number of  $S^{13+}$  ions, on the other hand, results in enhanced screening of the accelerating potential for the  $S^{12+}$  ions. Therefore, the  $S^{12+}$  ions have a slightly larger TOF value at resonance, as compared to TOF values obtained at the off-resonance electron energies (see Figure 2b). This effect, however, does not influence the total abundance of the ion bunch and thus it is not significant for the determination of the recombination rates.

The ion intensities were extracted from the TOF spectra by integrating the corresponding measured charge state peaks (see e.g. Figure 2a). It is observed that the baseline for TOF spectrum goes below zero at several points. This effect has a technical origin: it seems that internal voltages applied to the dynodes in the detector drop with high count rate and the re-charge current pulls the baseline down. The non-constant baseline induced individual offsets for the charge state populations and was corrected. In order to find the area of the peaks the base line was determined at the start and end of the peaks by taking an average of 30-40 points for better statistics. Using these averaged values at the start and end of the peaks, the slope of the baseline was determined. The peak areas were obtained by integration using this baseline. We made sure in the analysis that a negative baseline does not affect the peak areas during integration.

The extracted ion intensities of the five highest charge states as a function of the electron energy are shown in Figure 3. By monitoring these intensities, the DR resonances at a particular electron energies are identified as a decrease of the intensity of the mother ions with a simultaneous increase of the intensity of the daughter ions. For example the gain in the Li-like ions is evenly balanced by the loss of the He-like ions. This was the case for all resonances in all charge states except for the H-like ions. The gain in the intensity of He-like ions was twice as high as the corresponding loss of the H-like ions. The most probable reason for this discrepancy was a loss of  $S^{15+}$  and  $S^{16+}$  ions in the TOF beam line. The beam line contains a dipole magnet with a remnant magnetic field which deflected and thus reduced the transmission of H-like ions by 50 %. The deflection for lower charge states was smaller and did not affect the ions hitting the detector. We corrected for this effect. The accuracy of this correction was verified by the measured x-ray intensities of K-shell RR into  $S^{16+}$  and  $S^{15+}$  ions. The ratio of the populations of  $S^{16+}$  and  $S^{15+}$  ions derived from the x-ray measurement was 2.84, as compared to 2.82, derived from the corrected TOF data.

The sum of the ion intensities formed a smooth curve as a function of the electron energy (Figure 3, top panel). It indicated linearity of the detector's response within  $\pm 6\%$  to the number of ions. An abrupt change in the number of ions due to DR resonances would induce variation in the summed intensity at all resonances if the detector's response was not linear. There is a dip in the summed intensity in the energy range 1.75-1.9 keV where DR resonances for  $S^{15+}$  and  $S^{14+}$  ions are observed. This dip is visible in the spectra of all ions i.e. from  $S^{16+}$  to  $S^{13+}$  ions (see figures 2b and 3), although there is no DR for  $S^{16+}$  (bare) ions. Around 2.3 keV there is for example an increase in  $S^{14+}$  and  $S^{13+}$  ions but there is no dip in the summed plot. We conclude from these considerations that the dip is most probably due to a reduced trapping efficiency for all ions (by e.g. a variation of the electron beam space charge potential) at that energy and this is accounted for in the normalization. However, an uncertainty due to a very small variation in the summed data plot is taken into account as systematic error. As the detector's response is linear, the ion intensities can be used in rate equations instead of number of ions.

The spectrum of  $S^{15+}$  ions features an interesting peak at  $\approx 2.15$  keV (see Figure 3). This is astonishing, because the incident electron energy is not sufficient for direct EII of He-like ions (3.223 keV). One possible reason for this peak could be resonant excitation and double autoionization of He-like sulfur ions initially in a metastable state. However, without a calculation supporting this assumption at this time, we choose to leave the identification of the process for a later time.

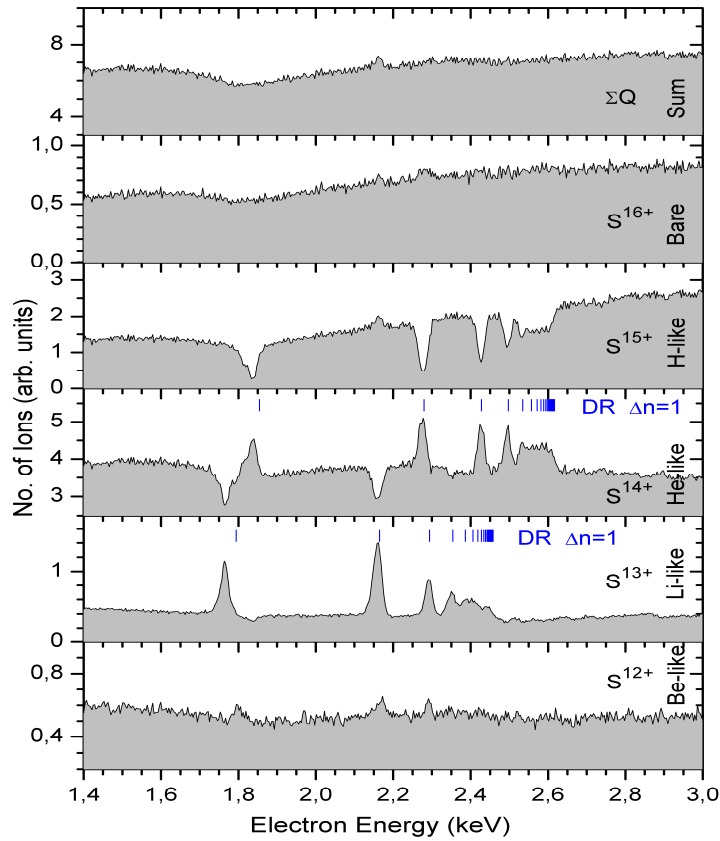


Figure 3. Number of sulfur ions of various charge states at the end of the probing time as a function of the probing electron energy. The top panel is the sum of spectra for these charge states. The vertical bars denote estimated DR resonance energy positions obtained with equation 1.

The charge state dynamics of the ions in EBIT is described by a set of coupled rate equations (Penetrante et al. 1991; Lu & Currell 2009), which contain the numbers of ions in different charge states and the rates of the charge changing processes (EII, RR, DR, and charge exchange). The ion intensities before and after the probing time were used as boundary conditions for solving the rate equations. By subtracting the background due to RR and charge exchange and normalizing the result to the electron density, the DR rate coefficients are obtained as shown in Figure 4. In the rate equations for He-like sulfur the feeding term due to EII of Li-like sulfur is included. For S XIV the ionization data, in the energy range 1-3 keV, from Dere 2007 is 4-12% higher than from Lennon et al. 1988. The ionization data from Dere 2007 is based on the most recent measurements and calculations using the FAC code. The measured ionization cross sections for Li-like isoelectronic sequence e.g. Si XII and Cl XV (close to S XIV) are also reported. The estimated error is 10-30%. The ionization data from Lennon et al 1988 is based on Coulomb Born approximation. They reported an estimated error of 40-60% in cross sections for sulfur ions. Therefore the required EII cross sections are taken from (Dere 2007). In the data analysis, the overlap between the electron beam and the ion cloud is estimated, using the EII data for H-like ions, and found to be comparable to previous measurements at an EBIT device (Porto et al. 2000). Since our EBIT has a similar configuration an averaged overlap factor, varying with the probing energy, is then used in the analysis.

The error in the rate coefficients is dominated by the systematic error which is estimated to be 19% in total at a confidence level of one sigma. It arises from uncertainties in the electron beam current (2%), radius of the electron beam (4%), the electron beam and ion cloud overlap factor (10%), ion extraction and transport efficiency (10%), and ion detection efficiency (10%). The 1-sigma statistical error is estimated to be 3-6%. In the rate coefficients of He-like sulfur, there is also an uncertainty due to the effect of the abundance of He-like ions caused by EII of Li-like ions. Since the ratio of Li-like to He-like ions is approximately 1/8 and since the dominating process in the charge balance equations for He-like ions is DR, the uncertainty in the EII data has only a minor effect on the uncertainty of the He-like rate coefficients. We estimate this uncertainty to 8% by using EII data from the literature (Dere 2007). Therefore total error for He-like case is 21%.

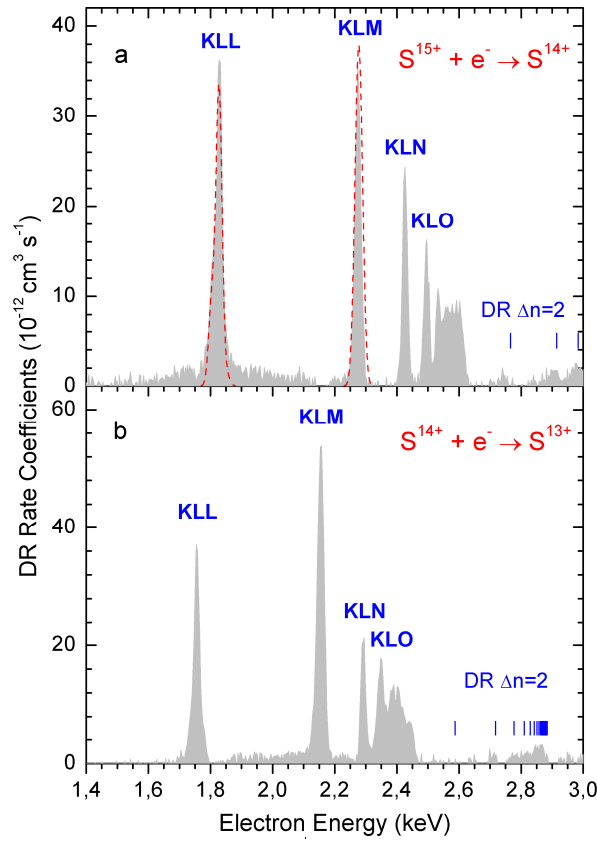


Figure 4. DR rate coefficients for  $S^{15+}$  (a) and  $S^{14+}$  (b) ions are shown as a function of the electron energy. Experimental results are marked by gray areas and the dotted red line represents calculations obtained from RMBPT. Auger notation is used for labeling  $\Delta n=1$  DR resonance groups. The estimated DR positions for  $\Delta n=2$  resonance are shown by vertical bars.

The experimental results for H-like ions were compared with advanced calculations. The DR resonance strengths are calculated with a method based on relativistic many-body perturbation theory (RMPBT) (Tokman et al. 2002). To describe the autoionizing states of KLL and KLM type in  $S^{14+}$ , the method of complex rotation is employed, which includes the coupling to the continuum. A doubly excited autoionizing state is hereby characterized by a complex energy eigenvalue, where the imaginary part gives its autoionization half-width and the real part its energy position. The radiative transition rates are evaluated in the dipole approximation. The strengths of the DR resonances are obtained using the calculated resonance position, and the radiative and Auger rates of the doubly excited states. The DR cross sections are then calculated from the resonance strengths, assuming for every resonance a Lorentzian profile distributed around the resonance position and with the width given by the natural width of the doubly excited-state. The DR rate coefficients are finally obtained by convoluting the cross sections times average electron velocity with a Gaussian, representing the electron beam energy distribution. The width of the electron beam is 24 eV, obtained from the fitting of a resonance (Ali et al. 2011a).

The DR rate coefficients for  $S^{15+}$  and  $S^{14+}$  ions as a function of the electron energy are shown in Figure 4 a and b, respectively. DR associated with the excitation of a K shell electron to the L shell during the attachment of a free electron ( $\Delta n=1$  type DR), gives rise to a series of strong peaks labelled in Figure 4 using the Auger notation. Additionally, at higher energies,  $\Delta n=2$  type DR resonances are also observed, associated with the excitation of a K shell electron to the M shell. The notation  $\Delta n$  corresponds to a change of the principal quantum number of the excited core electron. The dashed lines in Figure 4a represent the calculations for H-like sulfur obtained from RMBPT. The theory agrees well with the experiment in both the position of the resonances and their absolute strength.

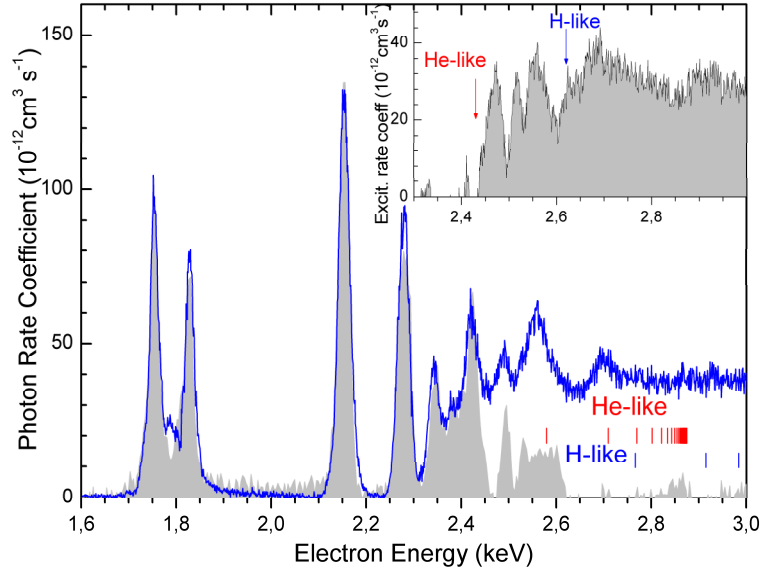


Figure 5. The photon rate coefficients obtained from TOF and x-ray measurements are shown as a function of the electron energy. The gray area is obtained from experimental TOF DR rates and the solid line shows those from x-ray emission. The vertical bars show estimated resonance positions associated with  $\Delta n=2$  DR. The inset graph shows excitation rate coefficients of H-like and He-like sulfur and has same energy scale. The K to L excitation threshold positions are denoted by vertical arrows.

In addition to the measurement of the extracted ion abundances we also measured the photons in the energy range of 1-7 keV, emitted from the trapped ions (Ali et al. 2011a). This enables us to check the consistency of both measurements (X ray and TOF) and we can get additional information by comparing the results. The TOF measurements give the DR part for the individual charge states, whereas the x-ray measurement detects photons that are emitted as a result of recombination and EIE. Here the DR and EIE photons can not always be distinguished due to insufficient resolution of the x-ray detector. However, the combination of these two methods enables us to disentangle the photon spectrum of EIE from the photon spectrum of the charge changing processes.

The background-subtracted total photon yield in the photon energy range of 1-4 keV is displayed as a function of the electron energy in Figure 5 by the blue line (Ali et al. 2011a). The total photon yield was corrected for the photon energy-dependent detection efficiency, the anisotropy, and the solid angle. For comparison, the total photon rate was also obtained from the experimental total DR rates. For this, the number of H-like ions was calculated using the measured rate of K-shell RR photons, known electron density, and the theoretical K-shell RR cross section. The number of He-like ions was obtained using the experimental ratio of H- and He-like ions, derived independently from both the TOF and the x-ray spectra. The contribution from the less abundant lower charge states to the photon spectrum was insignificant. Every recombination into a H-like ion produces two K X rays in contrary to the lower charge states and this factor two was taken into account. In H-like ions there is only one electron in the K shell. In case of DR an incident electron is captured and simultaneously the core electron is excited from K to higher shell. There are two vacancies in the K shell so two K X rays are produced in this case of DR (Schulz et al. 1987). The intensities of the radiative transitions due to DR were summed up. The total calculated photon yield is shown in Figure 5, grey area.

The agreement of the photon rate coefficients obtained from both methods is remarkable in the energy range of the DR resonances (up to 2.4 keV), which demonstrates the consistency of our measurements. For electron energies above 2.4 keV (see Figure 5) the photon rate coefficients from x-ray measurements are higher than from TOF, since x ray measurements contain photons as a result of DR and EIE, whereas TOF method gives only the DR part. This allows us to extract the EIE rate coefficients from the difference of both spectra, as shown in Figure 5 (inset graph). The thresholds for excitation obtained from the NIST atomic database (Ralchenko et al. 2011) are indicated by vertical arrows in the inset of Figure 5. They agree well with the onsets of x-ray intensities in the difference spectrum. The vertical bars in the main part of Figure 5 show the estimated resonance positions associated with  $\Delta n=2$  DR. A small recombination rate is seen at these  $\Delta n=2$  resonances in the TOF spectrum. As evident from this comparison of data from the two techniques, such weak recombination resonances can only be seen in TOF spectra, while in the x-ray data these are swamped by the EIE-induced x-ray background. With this technique the EIE rates can be obtained only for the cocktail of

the trapped ions. However, by varying and measuring the trapped ions charge state distribution, this method would enable to extract EIE rate coefficients for specific charge states, and thus has good prospects for further studies of EIE at EBITs.

The first measurement of  $\sigma^{\text{EIE}}$  on EBIT was done by Marrs et al. 1988 using a Si(Li) detector and a crystal spectrometer without taking into account polarization effect. In the following measurements this effect was accounted for, and high-purity Ge detectors, and microcalorimeters, as well as, crystal spectrometers were used (see e.g. Chen & Beiersdorfer 2008). As  $\sigma^{\text{RR}}$  is much smaller than  $\sigma^{\text{EIE}}$ , approximately one RR photon is observed for 100-1000 photons in the EIE lines. In comparison to this, the combination of TOF and x-ray measurements with low resolution, highly efficient photon detection is much faster. It is also independent of any line identifications using calculations that are necessary in the high-resolution method. The method can be improved by measuring the photons with efficient next-generation X-ray microcalorimeters and also detecting the extracted ions as discussed here.

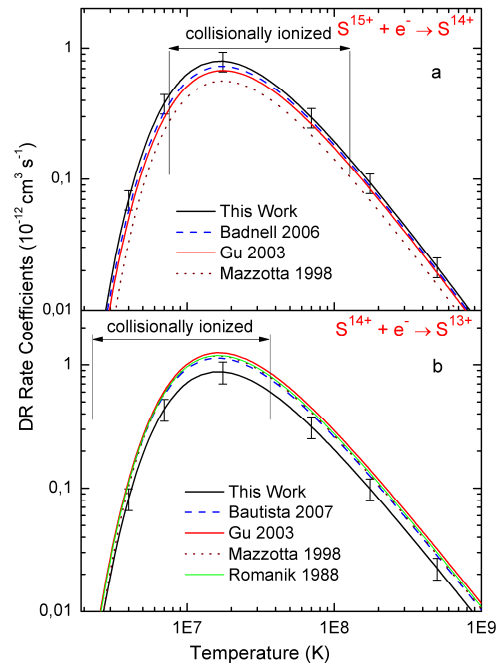


Figure 6. Plasma rate coefficients of  $S^{15+}$  (a) and  $S^{14+}$  (b) ions are shown as a function of temperature. The calculated data from the literature is shown for comparison. The error bars show uncertainties in our results which are estimated to be 19% for H-like and 21% for He-like sulfur. The temperature ranges are indicated, for which the abundances of the respective ion is higher than 10% of the maximum occurrence in collisionally ionized plasma (Bryans et al. 2009).

The modelling and diagnostics of plasmas require DR rate coefficients as a function of plasma temperature. These temperature-dependent rate coefficients are obtained by convoluting the experimental energy-dependent DR rate coefficients, with a Maxwell-Boltzmann electron energy distributions (Savin 1999). This folding is valid, if the energy spread of the electron beam is much smaller than the electron energy-spread in the plasma (Schippers et al. 2001). The derived plasma rate coefficients for  $S^{15+}$  and  $S^{14+}$  ions are shown in Figure 6a and 6b, respectively. The displayed ranges indicate temperatures at which the abundances of the respective ion is higher than 10% of the maximum occurrence in collisionally ionized plasma (Bryans et al. 2009).

The plasma DR rate coefficients for H-like sulfur agree well with the published theoretical values (Mazzotta et al. 1998; Gu 2003; Badnell 2006). For He-like sulfur, on the other hand, the recent calculations (Bautista & Badnell 2007) overestimate the DR rate coefficients by 23 %. The older calculations give even higher predictions (Romanik 1988; Mazzotta et al. 1998; Gu 2003). This discrepancy might be due to a more complicated structure of the resonances in the Li-like ion which generally have three open shells and thus are harder to represent well in a calculation as compared to the doubly excited states in the two-electron system needed for recombination of the H-like system. Theory is thus very differently reliable for different atomic systems. Moreover, note that the experimentally derived rate coefficients for both H-like and He-like sulfur are closer to the latest calculations (Badnell 2006; Bautista & Badnell 2007).

#### 4. CONCLUSIONS

Dielectronic recombination and electron impact excitation rate coefficients have been measured for astrophysically relevant sulfur ions. A time-of-flight technique was used to monitor the charge distribution of the extracted ions. It allowed us to obtain the DR rate coefficients individually for H-like and He-like ions. They were cross checked by the photon resolved measurement. While the photon-resolved studies were not charge-sensitive, they enabled us to extract pure electron impact excitation rates for the known charge state distribution of the ions. The calculated rates for H-like ions agree well with the experimental findings. The temperature-dependent rate coefficients were also derived. Up to now they were known only theoretically. For H-like ions they agree with the literature values. However, for He-like ions the experimental rate coefficients seem to be around 20 % lower than the literature values.

#### ACKNOWLEDGMENTS

We acknowledge financial support from the Knut & Alice Wallenberg Foundation and the Swedish Research Council VR. S. M. and S. A. are grateful to the Higher Education Commission of Pakistan for financial support via the Swedish Institute.

#### REFERENCES

- Ali, R., Bhalla, C. P., Cocke, C. L., & Stockli, M. 1990, *Phys. Rev. Lett.*, 64, 633
- Ali, S., Mahmood, S., Orban, I., Tashenov, S., Li, Y. M., Wu, Z., & Schuch, R. 2011a, *J. Phys. B: At. Mol. Opt. Phys.*, 44, 225203
- Ali, S., Mahmood, S., Orban, I., Tashenov, S., Li, Y. M., Wu, Z., & Schuch, R. 2011b, *JINST*, 6, C01016
- Anders, E., & Grevesse, N. 1989, *Geochim. et Cosmochim. Acta*, 53, 197
- Arnaud, K. A. in *Astronomical Data Analysis Software and Systems V*, ed. by G. Jacoby, J. Barnes, vol. 101 (ASP, Syracuse, 1996), p. 17
- Badnell, N. R. 2006, *A&A*, 447, 389
- Bautista, M. A., & Badnell, N. R. 2007, *A&A*, 466, 755
- Biedermann, C., Radtke, R., & Fussmann, G. 1997, *Phys. Rev. A*, 56, R2522
- Boroson, B., Vrtilik, S. D., Kallman, T., & Corcoran, M. 2003, *ApJ*, 592, 516
- Böhm, S., Enulescu, A., Fritioff, T., Orban, I., Tashenov, S., & Schuch, R. 2007, *J. Phys. Conf. Ser.*, 58, 303
- Bryans, P., Badnell, N. R., Gorczyca, T. W., Laming, J. M., Mitthumsiri, W., & Savin, D. W. 2006, *ApJS*, 167, 343
- Bryans, P., Landi, E., & Savin, D. W. 2009, *ApJ*, 691, 1540
- Burgess, A., & Summers, H. P. 1969, *ApJ*, 157, 1007
- Chen, H., & Beiersdorfer, P., 2008, *Can. J. Phys.*, 86, 55
- Clayton, D. 1983, *Principles of stellar evolution and nucleosynthesis*, University of Chicago Press
- Decourchelle, A., Sauvageot, J. L., Audard, M., Aschenbach, B., Sembay, S., Rothenflug, R., Ballet, J., Stadlbauer, T., & West, R. G. 2001, *A&A*, 365, L218
- Dere, K. P. 2007, *A&A*, 466, 771
- Dere, K. P., Landi, E., Young, P. R., Zanna, G. D., Landini, M., & Mason H. E. 2009, *A&A*, 498, 915
- DeWitt, D. R., Schneider, D., Clark, M. W., Church, D., & Chen, M. H. 1991, *Phys. Rev. A*, 44, 7185
- Dubau, J. & Volonte, S. 1980, *Rep. Prog. Phys.*, 43, 199
- Ferland, G. J., Korista, K. T., Verner, D. A., Ferguson, J. W., Kingdon, J. B. & Verner, E. M. 1998, *Publ. Astron. Soc. Pacific*, 110, 761
- Foster, A. R., Smith, R. K., Brickhouse, N. S., Kallman, T. R. & Witthoeft, M. C. 2010, *Space Sci. Rev.*, 157, 135
- Fujimoto, R., et al. 1995, *Publ. Astron. Soc. Japan*, 47, L31
- Gabriel, A. H. & Jordan, C. 1973, *ApJ*, 186, 327
- Grevesse, N., & Sauval, A. J. 1998, *Space Sci. Rev.*, 85, 161
- Gu, M. F. 2003, *ApJ*, 590, 1131
- Henley, D. B., Corcoran, M. F., Pittard, J. M., Stevens, I. R., Hamaguchi, K., & Gull, T. R. 2008, *ApJ*, 680, 705
- Hobein, M., Orban, I., Böhm, S., Solders, A., Suhonen, M., Fritioff, T., Tashenov, S., & Schuch, R. 2010, *JINST*, 5, C11003

- Iaria, R., AI', A. D., Lavagetto, G., Salvo, T. Di., Robba, N. R., & Burderi, L. 2008, *ApJ*, 673, 1033
- Kallman, T. R., & Palmeri, P. 2007, *Rev. Mod. Phys.* 79, 79
- Khan, J. I., Harra-Murnion, L. K., Hudson, H. S., Lemen, J. R., & Sterling, A. C. 1995, *ApJ*, 452, L153
- Kilgus, G., et al. 1990, *Phys. Rev. Lett.*, 64, 737
- Knapp, D. A., Marrs, R. E., Levine, M. A., Bennett, C. L., Chen, M. H., Henderson, J. R., Schneider, M. B., & Scofield, J. H. 1989, *Phys. Rev. Lett.*, 62, 2104
- Lennon, M. A., Bell, K. L., Gilbody, H. B., Hughes, J. G., Kingston, A. E., Murray, M. J., & Smith, F. J. 1988, *J. Phys. Chem. Ref. Data*, 17, 1285
- Levine, M. A., et al. 1989, *Nucl. Instr. Method Phys. B*, 43, 431
- Lu, X., & Currell, F. J. 2009, *Phys. Rev. ST Accel. Beams*, 12, 014401
- Marrs, R. E., Levine, M. A., Knapp, D. A., & Henderson, J. R. 1988, *Phys. Rev. Lett.*, 60, 1715
- Marshall, H. L., Canizares, C. R., & Schulz, N. S. 2002, *ApJ*, 564, 941
- Mazzotta, P., Mazzitelli, G., Colafrancesco, S. & Vittorio N. 1998, *A&AS*, 133, 403
- Miceli, M., Decourchelle1, A., Ballet, J. Bocchino, F., Hughes, J. P. Hwang, U. & Petre R. 2006, *A&A*, 453, 567
- Müller, A. J. 2009, *J. Phys. Conf. Ser.*, 194, 012002
- Orban, I., Tashenov, S., Ferro, F., Lindroth, E., and Schuch, R. to be submitted
- Penetrante, B. M., Bardsley, J. N., DeWitt, D., Clark, M., & Schneider, D. 1991, *Phys. Rev. A*, 43, 4861
- Porquet, D., Mewe, R., Dubau, J., Raassen, A. J. J., & Kaastra, J. S. 2001, *A&A*, 376, 1113
- Porquet, D., Dubau, J., & Grosso, N. 2010, *Space Sci. Rev.*, 157, 103
- Porto, J. V., Kink, I., & Gillaspay, J. D. 2000, *Rev. Sci. Instrum.*, 71, 3050
- Postberg, F., Kempf, S., Srama, R., Green, S. F., Hillier, J. K., McBride, N., & Grün, E. 2006, *Icarus*, 183, 222
- Ralchenko, Yu., Kramida, A.E., Reader, J., & NIST ASD Team (2011). NIST Atomic Spectra Database (ver. 4.1.0), (Online available: <http://physics.nist.gov/asd>) (2012, February 20).
- Romanik C. J. 1988 , *ApJ*, 330, 1022
- Savin, D. W. 1999, *ApJ*, 523, 885
- Sarazin, C. L. X-ray emission from clusters of galaxies, Cambridge University Press 1988
- Schippers, S., Müller, A., Gwinner, G., Linkemann, J., Saghir, A. A., & Wolf, A. 2001, *ApJ*, 555, 1027
- Schulz, M., Justiniano, E., & Schuch, R. 1987, *Phys. Rev. Lett.*, 17, 1734
- Schuch, R., Lindroth, E., Madzunkov, S., Fogle, M., Mohamed, T., & Indelicato, P. 2005, *Phys. Rev. Lett.*, 95, 183003
- Schuch, R., & Böhm, S. 2007, *J. Phys. Conf. Ser.*, 88, 012002,
- Smith, R. K., Brickhouse, N. S., Liedahl, D. A., & Raymond, J. C. 2001, *ApJ*, 556, L91
- Smith, R. K., & Foster, A.R., 2010, <http://www.atomdb.org>.
- Sterling, A. C., Hudson, H. S., & Watanabe, T. 1997, *ApJ*, 479, L149
- Summers, H. P. 2010, *The ADAS User Manual*, <http://www.adas.ac.uk>.
- Tokman, M., Eklöv, N., Glans, P., Lindroth, E., Schuch, R., Gwinner, G., Schwalm, D., Wolf, A., Hoffknecht, A., Müller, A. & Schippers, S., 2002, *Phys. Rev. A*, 66, 012703
- Watanabe, H., Currell, F. J., Kuramoto, H., Li, Y. M., Ohtani, S., Rourke, B. O., & Tong, X. M. 2001, *J. Phys. B: At. Mol. Opt. Phys.*, 34, 5095
- Watanabe, H., Tobiyama, H., Kavanagh, A. P., Li, Y. M., Nakamura, N., Sakaue, H. A., Currell, F. J., & Ohtani, S. 2007, *Phys. Rev. A*, 75, 012702
- Wojdowski, P. S., Liedahl, D. A., Sako, M., Kahn, S. M., Paerels, F. 2003, *ApJ*, 582, 959
- Wolf A 1992 Report MPI H-V15-1992 Max-Planck-Institut für Kernphysik Heidelberg
- Woosley, S. E., Heger, A., & Weaver, T. A. 2002, *Rev. Mod. Phys.*, 74, 1015
- Zhang, H., & Sampson, D. H. 1987, *ApJS*, 63, 487
- Zou, Y., Crespo López-Urrutia, J. R., & Ullrich, J. 2003, *Phys. Rev. A*, 67, 042703